

# Theory of the thermoelectricity of intermetallic compounds with Ce or Yb ions

V. Zlatić<sup>1</sup> and R. Monnier<sup>2</sup>

<sup>1</sup>*Institute of Physics, Bijenička cesta 46, P. O. Box 304, 10001 Zagreb, Croatia and*

<sup>2</sup>*ETH Hönggerberg, Laboratorium für Festkörperphysik, 8093 Zürich, Switzerland*

The thermoelectric properties of intermetallic compounds with Ce or Yb ions are explained by the single-impurity Anderson model which takes into account the crystal-field splitting of the  $4f$  ground-state multiplet, and assumes a strong Coulomb repulsion which restricts the number of  $f$  electrons or  $f$  holes to  $n_f \leq 1$  for Ce and  $n_f^{hole} \leq 1$  for Yb ions. Using the non-crossing approximation and imposing the charge neutrality constraint on the local scattering problem at each temperature and pressure, the excitation spectrum and the transport coefficients of the model are obtained. The thermopower calculated in such a way exhibits all the characteristic features observed in Ce and Yb intermetallics. Calculating the effect of pressure on various characteristic energy scales of the model, we obtain the  $(T, p)$  phase diagram which agrees with the experimental data on CeRu<sub>2</sub>Si<sub>2</sub>, CeCu<sub>2</sub>Si<sub>2</sub>, CePd<sub>2</sub>Si<sub>2</sub>, and similar compounds. The evolution of the thermopower and the electrical resistance as a function of temperature, pressure or doping is explained in terms of the crossovers between various fixed points of the model and the redistribution of the single-particle spectral weight within the Fermi window.

PACS numbers: 75.30.Mb, 72.15.Jf, 62.50.+p, 75.30.Kz,

## I. INTRODUCTION

The thermoelectric power,  $S(T)$ , of intermetallic compounds with Cerium and Ytterbium ions exhibits some characteristic features which allow the classification of these compounds into several distinct groups.<sup>1,2,3</sup> In the case of Cerium ions, the thermopower of the compounds belonging to the first group (type (a) systems) has a deep negative minimum at low temperatures<sup>1,2,4,5,6</sup> and a high-temperature maximum, typically between 100 K and 300 K. At the maximum,  $S(T)$  could be either positive or negative, as shown in Fig. 1. At very low temperatures, the type (a) systems order magnetically or become superconducting. The compounds of the second group (type (b) systems) have a negative low-temperature minimum and a positive high-temperature maximum but, in addition, the thermopower shows a smaller positive peak at lowest temperatures.<sup>1,7,8,9,10</sup> This second peak is sometimes concealed by a low-temperature phase transition; for example, in CeCu<sub>2</sub>Si<sub>2</sub> it becomes visible only in an external magnetic field which suppresses the superconducting transition,<sup>4</sup> and in CeRu<sub>2</sub>Ge<sub>2</sub> it shows up when the external pressure suppresses the magnetic transition.<sup>11</sup> The experimental evidence is now accumulating that the initial slope of the thermopower  $S(T)/T$  is positive for this class of (heavy fermion) materials, provided the measurements are performed at low enough temperature and with sufficient accuracy.<sup>6,7,8,12</sup> In the third group (type (c) systems), the low-temperature peak is well pronounced and shifted towards the high-temperature peak. The main difference with respect to the type (b) systems is that the sign-change of  $S(T)$  does not occur.<sup>13,14,15,16</sup> Finally, in some cases (type (d) systems) the thermopower grows monotonically towards the high-temperature maximum, and the low-temperature structure appears only as a shoulder on a broad peak, or is

not resolved at all.<sup>8,16,17,18</sup>

The clue to these various types of behavior comes from the high-pressure<sup>2,11,19,20,21</sup> and doping studies,<sup>1,14,16,24,25,26,27,28</sup> which show that the thermopower of Cerium compounds changes continuously from type (a) to type (d). A typical example is provided by the  $S(T)$  of CeRu<sub>2</sub>Ge<sub>2</sub>, which is plotted in Fig.1 as a function of temperature, for various pressures.<sup>11</sup> At ambient pressure, CeRu<sub>2</sub>Ge<sub>2</sub> is a type (a) system with a magnetic ground state and negative thermopower below 300 K. An increase of pressure leads to a thermopower with a small positive peak at low temperatures and an enhanced peak at high temperatures. A further increase of pressure enhances both peaks, shifts the low-temperature peak towards the high-temperature one, and makes the thermopower at intermediate temperatures less negative. For large enough pressure, the sign-change does not occur at all and for very high pressure the low-temperature peak merges with the high-temperature one, and transforms into a shoulder (see inset to Fig. 1). The high-temperature peak grows continuously but its position remains more or less constant, as  $S(T)$  changes from type (a) to (c). Eventually, for pressures above 10 GPa, the  $S(T)$  assumes the (d) shape. Here, the initial slope of  $S(T)$  decreases and the position of the maximum shifts to higher temperatures, but its magnitude does not change as pressure increases. Similar behavior is also seen in the high-pressure data of, CeCu<sub>2</sub>Si<sub>2</sub>,<sup>21</sup> CeCu<sub>2</sub>Ge<sub>2</sub>,<sup>20,22</sup> or CePd<sub>2</sub>Si<sub>2</sub>.<sup>23</sup> As regards doping, the substitutions which reduce the volume and make Ce ions less magnetic, transform  $S(T)$  from type (a) to type (b),<sup>24</sup> from (b) to (c),<sup>14,16</sup> or from (a) to (c),<sup>25,26,27</sup> while the substitutions which expand the volume and make the Ce more magnetic, transform the thermopower from, say, type (d) to type (c) or from type (c) to type (b).<sup>28</sup> This variation of shape is an indication that the local environment plays

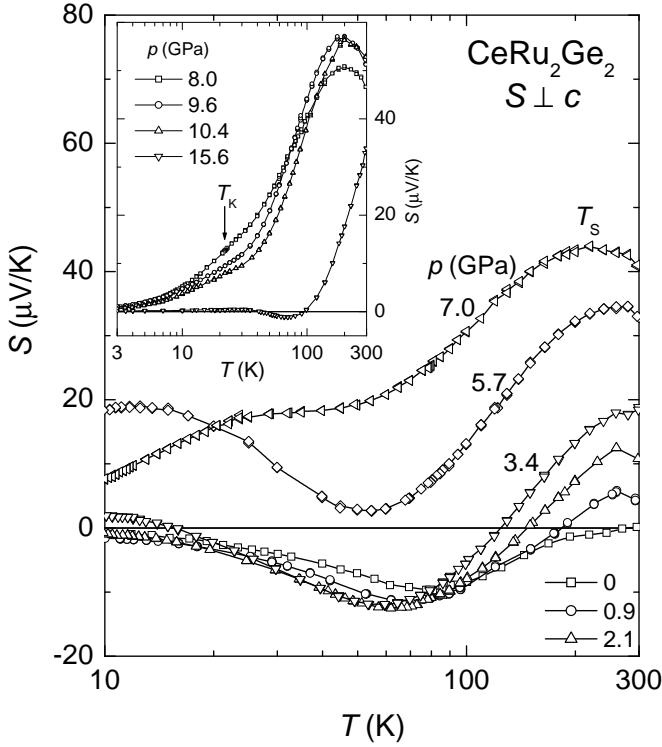


FIG. 1: Temperature dependence of the thermoelectric power  $S(T)$  of  $\text{CeRu}_2\text{Ge}_2$  for various pressures.  $T_K$  and  $T_S$  label the centre of broad, pressure-induced maxima, related to the Kondo effect and the crystalline electric field, respectively. The inset shows  $S(T)$  data of  $\text{CeRu}_2\text{Ge}_2$  in the non-magnetic phase.

an important role in determining the magnetic character of Ce and Yb ions. Even at high temperatures, where each  $4f$  ion is an independent scatterer, the thermopower of a sample with a high concentration of  $4f$  ions cannot be obtained by rescaling the low-concentration data.

The Ytterbium intermetallics can be classified using the mirror-image analogy with Cerium systems. This holds because the Yb ions fluctuate between  $4f^{13}$  and  $4f^{14}$ , while the Ce ions fluctuate between  $4f^1$  and  $4f^0$  configurations, and the dynamics of a single  $f$  hole and a single  $f$  electron is the same. A well-defined local moment leads in Yb systems to the type (a) behavior, such that the thermopower has a negative minimum at high temperatures and a positive maximum at low temperatures;<sup>29,30</sup> the size of the minimum is about the same as the size of the maximum. The thermopower of (b)-type Yb systems<sup>31,32,33</sup> mirrors the (b)-type Ce systems. Here, one finds two negative minima separated by a small positive maximum. The type (c) Yb systems have a nonmonotonic thermopower with a large (negative) minimum at high temperatures and a smaller one at low temperatures, but there is no sign-change.<sup>30,31,32,33</sup> Finally, the thermopower with a single negative peak centered around 100 K<sup>18,30,31,34</sup> mirrors the type (d) behavior of Ce systems. The reduction of volume by pressure

or doping<sup>30,33</sup> stabilizes the magnetic  $4f^{13}$  configuration of Yb ions, and transforms  $S(T)$  from, say, type (b) to type (a), from (c) to (b), or from (c) to (a).

The experimental results show that  $4f$  systems with similar thermopowers exhibit similarities in other thermodynamic<sup>35</sup> and transport<sup>37,38,39</sup> properties, and there is an obvious correlation between the shape of  $S(T)$  and the magnetic character of the  $4f$  ions. The thermopower measurements provide a simple and sensitive tool for characterizing the magnetic state of a  $4f$  ion in a given metallic matrix: the shape of  $S(T)$  changes from the (a)-type in the case of magnetic Ce (Yb) ions with stable  $f^1$  ( $4f^{13}$ ) configuration to the (d)-type for non-magnetic Ce (Yb) ions which fluctuate between the  $4f^1$  ( $4f^{13}$ ) and  $4f^0$  ( $4f^{14}$ ) configurations.

We explain the thermoelectric properties of Ce and Yb ions in terms of a single-impurity Anderson model which takes into account the splitting of the  $4f$  states by the crystalline electric field (CF), and assumes an infinitely large  $f$ - $f$  Coulomb repulsion, which restricts the number of  $f$  electrons or  $f$  holes to  $n_f \leq 1$  for Ce and  $n_f^{hole} \leq 1$  for Yb. We assume that pressure changes the coupling and the relative occupation of the  $f$  and conduction states, and impose the charge-neutrality constraint on the local scattering problem at each temperature and pressure. The total charge conservation provides a minimal self-consistency condition for a poor-man's treatment of pressure effects in stoichiometric compounds. The excitation spectrum of such a model in the vicinity of various fixed points, the crossovers induced by temperature and pressure, and the corresponding effects on  $S(T)$ , the number of  $f$  particles,  $n_f(T)$ , and the electrical resistance,  $\rho(T)$ , are calculated by the non-crossing approximation (NCA). The description of the stoichiometric compounds in terms of an impurity model is certainly inadequate at low temperatures where the  $f$  electrons become coherent. The errors due to such an approximation and the low-temperature errors inherent in the NCA calculations are discussed in detail at the end of Sec. II.

Our paper extends the long-standing theory of Coqblin,<sup>41,42</sup> which described the high-temperature properties of Ce and Yb intermetallics by the Coqblin-Schrieffer (CS) model with CF splitting, and its more recent version<sup>3</sup> which improved the low-temperature calculations by rescaling the coupling constants. These previous theories explained the main features of the temperature dependence of the thermopower<sup>3,42</sup> and the magnetic susceptibility<sup>35</sup> but could not describe the pressure effects, because the CS model neglects charge fluctuations. Furthermore, the approximations used to solve the effective high- and low-temperature models cease to be valid at temperatures at which  $S(T)$  changes sign,<sup>3</sup> such that the shape of  $S(T)$  between the two maxima (minima) in Ce (Yb) systems could only be inferred from an interpolation.

Here, we consider both the local *spin* and *charge* fluctuations, and provide the full description of the impurity problem at various pressures and temperatures,

from above the CF temperature to below the Kondo temperature, including the intermediate regime where  $S(T)$  changes sign. Our results explain the shapes (a) to (d) of the thermopower, which are found in the systems like  $\text{CeAl}_3$ ,<sup>9</sup>  $\text{CeRu}_2\text{Ge}_2$ ,<sup>11,40</sup>  $\text{CeCu}_2\text{Si}_2$ ,<sup>21</sup>  $\text{CeCu}_2\text{Ge}_2$ ,<sup>20,22</sup> or  $\text{CePd}_2\text{Si}_2$ ,<sup>23</sup> and the 'mirror-image' shapes found in systems like  $\text{YbNiSn}$ ,  $\text{YbInAu}_2$ ,  $\text{YbSi}$  or  $\text{YbCu}_2\text{Si}_2$ .<sup>30</sup> We also explain the pressure data like on  $\text{CeRu}_2\text{Ge}_2$ <sup>11</sup> or  $\text{CeCu}_2\text{Si}_2$ ,<sup>21</sup> and the chemical pressure data on  $\text{Ce}_x\text{La}_{1-x}\text{PdSn}$ <sup>27</sup> and  $\text{Ce}_x\text{La}_{1-x}\text{Ru}_2\text{Si}_2$ <sup>15</sup> or  $\text{YbCu}_2\text{Si}_2$ .<sup>33</sup>

The paper is organized as follows. In Sec. II we introduce the model, discuss its limitations, and describe the method of solution. In Sec. III we provide the results for the transport coefficients of Ce- and Yb-based intermetallics. In Sec. IV we discuss the effects of temperature and pressure on the spectral function, analyze the fixed-point behavior, and relate the shapes of the thermopower to the properties of elementary excitations. Sec. V, gives the summary and the conclusions.

## II. THEORETICAL DESCRIPTION

We model the intermetallic compounds by taking as many Ce or Yb ions per unit cell as required by the structure, but assuming that the scattering of conduction electrons on a given  $4f$  ion does not depend on other  $4f$  ions, except through the modification of the chemical potential. In other words, we consider an effective impurity model which treats the  $4f$  states as scattering resonances rather than Bloch states but take into account the charge transfer due to the local scattering and adjust the chemical potential,  $\mu$ , so as to maintain the overall charge neutrality of the compound. Such a description of the lattice problem applies at temperatures at which the mean free path of the conduction electrons is short and the scattering is incoherent. We consider mainly the Ce intermetallics and present only a few preliminary results for Yb intermetallics. The Cerium ions are allowed to fluctuate between the  $4f^0$  and  $4f^1$  configurations by exchanging electrons with the conduction band; the (average) energy difference between the two configurations is  $|E_f|$  and the hopping is characterized by the matrix element  $V$ . The  $4f^2$  configuration is excluded, i.e., an infinitely strong Coulomb repulsion  $U$  between  $f$  electrons is assumed. The  $4f^1$  configuration is represented by  $N$  crystal field levels: there are  $N - 1$  excited states separated from the CF ground level by energies  $\Delta_i \ll |E_f|$ , where  $i = 1, \dots, N - 1$ . The local symmetry is taken into account by specifying the respective degeneracies of these levels,  $\mathcal{N}_i$ . Thus, the low-energy excitations of Ce intermetallics are modeled by an effective single-impurity Anderson Hamiltonian,<sup>43</sup>

$$H_A = H_{band} + H_{imp} + H_{mix}, \quad (1)$$

where  $H_{band}$  describes the conduction band,  $H_{imp}$  describes the CF states, and  $H_{mix}$  describes the transfer

of electrons between  $4f$  and conduction states. In the absence of mixing, the conduction band is described by a semielliptical density of states,  $N(\epsilon)$ , centered at  $E_c^0$  and of half-width  $W$ , and the unrenormalized  $f$  states are represented by a set of delta functions at  $E_f^0$  and  $E_f^i = E_f^0 + \Delta_i$ . The conduction states and the  $f$  states have a common chemical potential, which is taken as the origin of the energy axis. The properties of the model depend in an essential way on the CF splittings and on the coupling constant  $g = \Gamma/\pi|E_f|$ , where  $\Gamma = \pi V^2 N(E_c^0)$  measures the coupling strength between the  $f$  electrons and the conduction band,  $E_f = \sum_{i=0}^{N-1} \mathcal{N}_i E_f^i / \mathcal{N}$ , and  $\mathcal{N} = \sum_{i=0}^{N-1} \mathcal{N}_i$  is the total degeneracy. We assume  $E_c^0 > 0$ ,  $E_f < 0$ , and  $\Gamma, \Delta_i \ll |E_f| \simeq W$ , i.e.,  $g \ll 1$ . Since a single  $f$  hole is dynamically equivalent to a single  $f$  electron, we obtain the results for Yb ions by performing the model calculations for a 8-fold degenerate  $f$  hole subject to the appropriate CF.

The  $g \ll 1$  limit of the Anderson model is controlled by several fixed points which are well understood.<sup>43</sup> In the case of a Ce ion with two CF levels split by  $\Delta$ , the fixed point analysis can be summarized as follows. At small coupling, such that  $\Gamma < \Delta \ll |E_f|$ , we find  $n_f(T) \simeq 1$  and the model exhibits the Kondo effect. That is, all the physical properties depend only on the Kondo temperature,  $T_0$ , which is uniquely determined by  $g$ ,  $\Delta$ , and the degeneracies of the CF states (for the NCA definition of  $T_0$  see Ref. <sup>43</sup> and Sec. IV below). The low-temperature behavior is characterized by the Fermi liquid (FL) fixed point, which describes a singlet formed by an antiferromagnetically coupled  $f$  electron and conduction electron. An increase of temperature breaks the singlet and gives rise, at about  $T_0$ , to a transition to the local moment (LM) fixed point, which describes a CF-split  $f$  state weakly coupled to the conduction band. The effective degeneracy of this  $f$  state is defined by the lowest CF level. For  $T > \Delta$ , there is a further crossover to another LM fixed point, which describes the scattering of conduction electrons on a fully degenerate local moment. At higher coupling, such that  $\Gamma \simeq 2\Delta \ll |E_f|$ , the  $f$  charge is reduced to  $0.8 < n_f(T) < 0.95$ , and the impurity still behaves as a Kondo ion, but the Kondo scale is much higher than in the case  $\Gamma < \Delta \ll |E_f|$ . The two LM regimes are now close together and the crossover from the FL to the LM regime occurs at temperatures which are comparable to  $\Delta$ . At very high coupling, such that  $2\Delta \leq \Gamma \ll |E_f|$  and  $n_f(T) \leq 0.8$ , the  $f$  ions appear to be non-magnetic at all accessible temperatures due to the mixing of the  $4f^0$  and  $4f^1$  configurations. In this valence fluctuating (VF) regime, the behavior is non-universal and changes slightly, when the calculations are performed for different sets of parameters. Away from  $n_f \simeq 1$ , more than one energy scale is needed to fully characterize the model. Other CF schemes pertinent to Ce and Yb ions in a different environment are characterized by similar fixed points.

Our calculations show that the functional form of the

response functions changes at the crossover and that the  $g \ll 1$  limit of the Anderson model captures all the main features of the experimental results on Ce and Yb intermetallics. To explain the pressure effects, which changes the thermopower of Ce and Yb systems in opposite ways, we assume that the exchange coupling  $g$  increases in Ce and diminishes in Yb compounds, as pressure increases. This difference arises because Ce fluctuates between  $4f^0$  and  $4f^1$ , while Yb fluctuates between  $4f^{14}$  and  $4f^{13}$  configurations, so that the pressure-induced reduction of the number of electrons in the  $f$ -shell makes Ce ions less magnetic and Yb ions more magnetic.

In Ce intermetallics, there is a substantial overlap between the  $f$  wave functions of Ce and those of the neighboring atoms, and we associate the pressure-induced increase of  $g \simeq \Gamma/|E_f|$  with an enhancement of the hybridization  $\Gamma$ . This enhances the Kondo temperature, and pushes the system from the Kondo to the VF limit. In stoichiometric compounds, the pressure-induced reduction of  $n_f$  is accompanied by the increase of  $n_c$ , because the total charge of a given compound,  $n_{tot} = n_c + n_f$ , is constant. The conservation of particles is enforced by adjusting  $\mu$ , and since all the energies are measured with respect to  $\mu$ , this amounts to shifting  $E_f$  and  $E_c$  by some amount  $\delta\mu(T, \Gamma(p))$ . Thus, we describe the pressure effects for a given Ce compound by changing  $\Gamma$  and keeping  $E_c - E_f$  constant. The changes in the band-width and the CF splitting are neglected.

In Yb intermetallics, the  $f$  states are more localized than in Ce systems, and we assume that the decrease in the radius of the  $4f$  shell as it loses charge at elevated pressure is sufficient to compensate for the increase in hybridization brought about by the reduction in unit cell volume. The reduction of  $g \simeq \Gamma/|E_f|$  in Yb compounds is achieved through an enhancement of the hole binding energy  $E_f$  as the neighbouring ions get closer to the rare earth, while  $\Gamma$  remains essentially constant. This reduces the Kondo temperature, and drives the system towards the Kondo limit. Since  $\Gamma$  is treated as a material-specific constant, we model the pressure effects in Yb systems by shifting  $E_f$  and solving for  $E_c$ , so as to preserve  $n_{tot}^{hole}$ . This procedure shifts  $E_f$  and  $E_c$  by different amounts and makes the separation  $E_c - E_f$  pressure dependent. However, when temperature is changed at constant pressure, the charge neutrality is enforced in the same way as for Ce compounds, by shifting the chemical potential without changing the separation  $E_c - E_f$ . The changes in the bandwidth and the CF splitting are neglected. Describing the pressure effects in such a way, we can calculate the response functions of the model for any value of the external parameters, and study the transitions between various fixed points.

The electrical resistivity and the thermopower of the single-impurity Anderson model are obtained from the usual expressions,<sup>44</sup>

$$\rho_{mag} = \frac{1}{e^2 L_{11}}, \quad (2)$$

$$S = -\frac{1}{|e|T} \frac{L_{12}}{L_{11}}, \quad (3)$$

where  $L_{11}$  and  $L_{12}$  are given by the static limits of the current-current and current-heat current correlation functions, respectively. In the absence of nonresonant scattering the vertex corrections vanish and the transport integrals can be written as,<sup>43,45,48</sup>

$$L_{ij} = \frac{\sigma_0}{e^2} \int_{-\infty}^{\infty} d\omega \left( -\frac{df(\omega)}{d\omega} \right) \tau(\omega) \omega^{i+j-2}, \quad (4)$$

where  $\sigma_0$  is material-specific constant,  $f(\omega) = 1/[1 + \exp(\omega/k_B T)]$  is the Fermi function,  $1/\tau(\omega)$  is the conduction-electron scattering rate,<sup>43</sup>

$$\frac{1}{\tau(\omega)} = cN\pi V^2 A(\omega), \quad (5)$$

$A(\omega) = \mp \frac{1}{2} \text{Im } G_f(\omega \pm i0^+)$  is the  $f$ -electron spectral function,  $G_f(z)$  is the Green's function, and  $c$  is the concentration of  $f$  ions. Eqs.(4) and (5) show clearly that the sign and the magnitude of  $S(T)$  are determined by the spectral weight within the Fermi window (F window), i.e., by the shape of  $A(\omega)$  for  $|\omega| \leq 2k_B T$ . The sign of  $S(T)$  is positive if the F window shows more states above than below the chemical potential, and is negative in the opposite case. The difficult part is to find  $G_f(\omega \pm i0^+)$  and, here, we solve this problem by the NCA, following closely Refs.<sup>43,47</sup>, where all the technical details can be found. The main difference with respect to these NCA calculations is that we take  $c = 1$  and enforce the overall charge neutrality.

A detailed comparison with the experimental data shows that the transport coefficients obtained from the single-impurity Anderson model have all the hallmarks of the experiments, but discrepancies appear at low temperatures. This indicates the limitations of our approach which should be considered before presenting the NCA results.

There are two main causes for the breakdown of the single-impurity model and the NCA calculations. First, at temperatures much below  $T_0$  the NCA spectral function develops an unphysical spike, such that the resistivity and the thermopower become artificially enhanced. This error becomes particularly severe at high pressure, because the characteristic scale  $T_0$  increases very rapidly with  $\Gamma$  and the non-analytic NCA spike appears at rather high temperatures. The unphysical enhancement of the low-frequency part of  $A(\omega)$  reduces the integral for  $L_{11}$ , which is strongly underestimated at low-temperature. The integral  $L_{12}$  is less affected by this pathology, because it has an additional  $\omega$  factor which removes the states within the Fermi window. Thus, the overall shape of  $S(T) \simeq L_{12}^{NCA}/L_{11}^{NCA}$  seems to be qualitatively correct, even though the low-temperature part of the curve has an unphysical enhancement. These difficulties are well known<sup>43</sup> and relatively easy to resolve in the Kondo

limit, where the model has a unique low energy scale,  $T_0$ . We can find  $T_0$  in the LM regime, where the NCA is reliable, and infer the low-temperature behavior from the universal power laws which hold in the FL regime. Combining the NCA results and FL theory, we can discuss the experimental data at all temperatures at which the single-ion approximation holds.

A more serious problem is that, in stoichiometric compounds, the  $f$  electrons become coherent at low enough temperatures. This leads to a magnetic transition in  $\text{CeRu}_2\text{Ge}_2$ , the formation of a heavy FL in  $\text{CeRu}_2\text{Si}_2$ , superconductivity in  $\text{CeCu}_2\text{Si}_2$ , or some more complicated ground states. At high pressure, the coherence sets in at very high temperatures, as revealed by low values of the electrical resistance. The onset of coherence (like the NCA pathology) has its main impact on the low-energy states, giving  $L_{11}^{\text{lattice}} \gg L_{11}^{\text{impurity}}$ , so that the impurity result badly overestimates the low-temperature electrical resistance. However, the considerations for the periodic Anderson model<sup>48</sup>, or other models with on-site correlation<sup>49</sup>, show that the integral for  $L_{12}$  also contains an additional  $\omega$  factor which reduces the contribution of the low-energy coherent states to  $L_{12}$ , like in the single impurity case. Thus, our results for  $S(T)$  provide a qualitative description of the experimental data at temperatures well below the onset of coherence, but the calculated values of  $S(T)$  around  $T_0$  are overestimated.

We mention also that the analysis of the doping effects in terms of "chemical pressure" is not complete, because doping might give rise to a charge transfer or change the character of the ground state, and that the mirror-image analogy between Ce and Yb systems holds for the resonant scattering but may be lost in the presence of any additional scattering channel. Despite these drawbacks, the NCA solution of the Anderson model provides a surprisingly accurate description for a large body of experimental data above the magnetic or superconducting transition temperature, and at low to moderate pressure.

### III. THERMOELECTRIC POWER RESULTS

In this section we present the NCA results for the transport coefficients, describe the thermopower and the electrical resistance due to Ce ions in some detail, show the results for the  $f$  occupation, present a few preliminary results for the thermopower of Yb, and compare our results with the experimental data.

Our strategy for Ce intermetallics is to illustrate the behavior of one particular compound as a function of temperature at various pressures. The compound is characterized at ambient pressure and high temperature by an initial parameter set  $\{W, E_c^0, N, \Gamma, E_f^0, \Delta_i, \mathcal{N}_i\}$ , where  $E_c^0 > 0$  and  $E_f^0 < 0$  are measured with respect to  $\mu$  and the high-temperature limit is defined by temperature  $k_B T_\Delta = \Delta_{N-1}$ . For given values of  $\Gamma$  and  $E_c^0 - E_f^0$ , we start the calculations at  $T = T_\Delta$  and find  $\delta\mu(T_\Delta, \Gamma)$  such that the total charge is the same as the one obtained

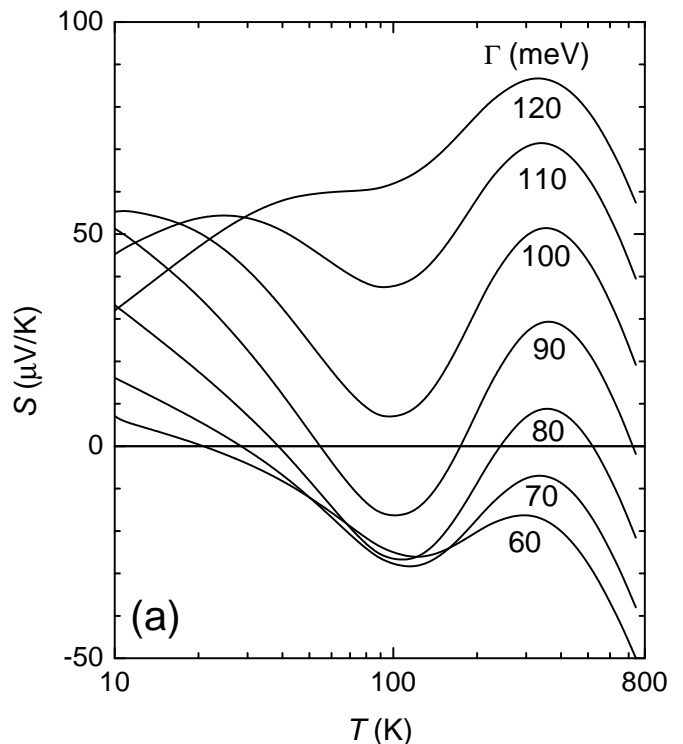


FIG. 2: Thermopower of Ce ions calculated by the NCA for the CF splitting  $\Delta = 0.07$  eV is plotted as a function of temperature for several values of the hybridization strength  $\Gamma < 2\Delta$ , as indicated in the figure. The bottom curve,  $\Gamma=0.06$  eV, corresponds to ambient pressure.

for  $\Gamma = 0$ . (In the absence of coupling we have  $n_f = 1$  and obtain  $n_c$  by integrating the unperturbed density of states.) At high temperatures, the  $f$ -state is almost decoupled from the conduction band, the renormalization of the parameters is small, and the numerics converge very fast. We then reduce the temperature, find the new shift  $\delta\mu(T, \Gamma)$  ensuring the charge conservation, and calculate the response functions for the resulting values of  $E_c$  and  $E_f$ . This process is continued until the NCA equations break down at  $T \ll T_0$ . To model the same system at different pressure, we change  $\Gamma$ , find again  $\delta\mu(T_\Delta, \Gamma)$ , and repeat the same procedure as at ambient pressure for  $T < T_\Delta$ . Note,  $n_{\text{tot}}$  and  $E_c - E_f$  are conserved at all temperatures and pressures.

As a numerical example we consider a semielliptical conduction band of half-width  $W = 4$  eV, centered at  $E_c^0 = 0.7$  eV, and a  $f$  state split into a doublet and a quartet<sup>46</sup> by the CF with  $\Delta = 0.07$  eV. We take  $n_{\text{tot}} = n_c + n_f = 5.6301$  electrons per ion (0.9383 electrons for each one of  $\mathcal{N}$  'effective spin' channels). The transport coefficients are calculated for the hybridization strength changing from 0.06 eV to 0.20 eV, i.e., for  $\Gamma$  varying from  $\Gamma < \Delta$  to  $\Gamma > 2\Delta$ . The single-particle excitation spectra corresponding to these parameters are discussed in Sec. IV.

Using the procedure outlined above we obtain for  $S(T)$

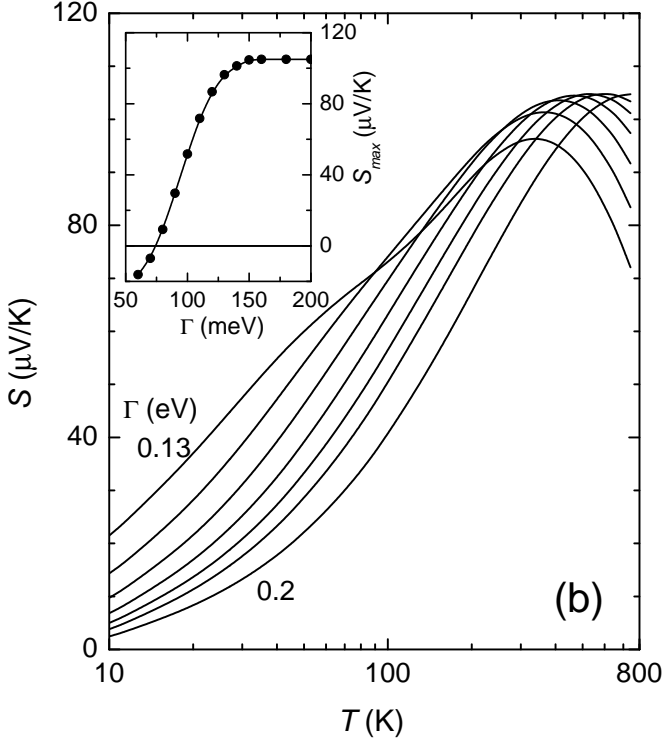


FIG. 3: Thermopower calculated by the NCA for the CF splitting  $\Delta = 0.07$  eV is plotted as a function of temperature for several large values of the hybridisation strength  $\Gamma$ , increasing from 0.13 eV to 0.2 eV. The bottom curve,  $\Gamma=0.20$  eV, is for the highest pressure. The inset shows the high-temperature maximum of  $S(T)$ , plotted as a function of  $\Gamma$ .

the results shown in Figs. 2 and 3. The calculated curves exhibit all the shapes (a) to (d) found in the experiments and give  $S(T)$  of the right magnitude, except at low temperatures where the calculated peak is too large with respect to the experimental data. As discussed already, the reason for this discrepancy is that the NCA overestimates the Fermi-level scattering rate for  $T \ll T_0$ , and that we neglected the coherent scattering, which sets in at temperatures of the order of  $T_0$ . Thus, our low-temperature result for  $L_{11}$  is artificially reduced, which makes  $S(T)$  too large. The sign and the topology of the  $S(T)$  curves do not seem to be affected by this error.

For  $\Gamma \leq \Delta$ , we have  $T_0 < 5$  K and  $n_f \geq 0.95$ , and obtain  $S(T)$  with two well separated peaks, as shown by the  $\Gamma=60$  and  $\Gamma=70$  meV curves in Fig. 2. The high-temperature peak is centered at  $T_S \simeq T_\Delta/2$  and for our choice of parameters  $S_{\text{max}} = S(T_S) < 0$ . The low-temperature maximum is at about  $T_0 \ll T_S$  and  $S_0 = S(T_0) > 0$ . The thermopower between the two maxima is mainly negative. Since most of the type (a) and (b) systems order magnetically or become superconducting above  $T_0$ , the low-temperature peak is not shown in Fig. 2 for  $\Gamma \leq 100$  meV. A small increase of  $\Gamma$  (due to, say, an increase of pressure) reduces  $n_f$  (see Fig. 4), enhances  $T_0$  and  $S_{\text{max}}$ , and expands the temperature range

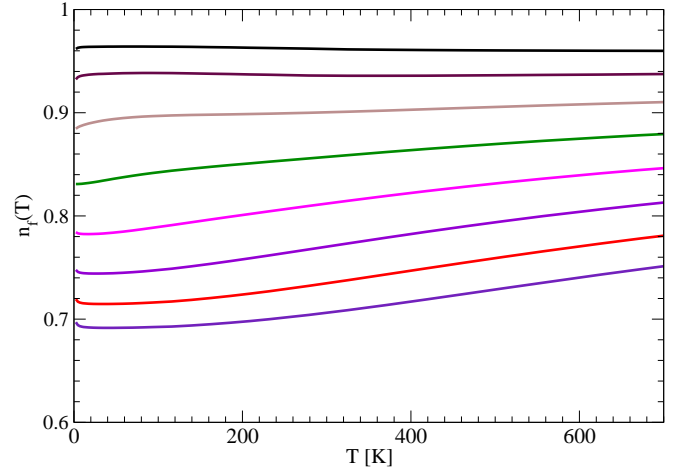


FIG. 4: f-electron number,  $n_f$ , calculated by the NCA for the CF splitting  $\Delta = 0.07$  eV is plotted as a function of temperature for several values of the hybridisation strength  $\Gamma$ . For the uppermost curve  $\Gamma=0.06$  eV and then it increases in steps of 0.02 eV. At the bottom curve  $\Gamma=0.20$  eV.

in which  $S(T)$  is positive. Such a behavior, which is typical of Kondo systems with small  $T_0$ , is in a qualitative agreement with the thermopower of the type (a) systems described in Sec. I, and with the data on  $\text{CeRu}_2\text{Ge}_2$ <sup>11</sup> at low pressures (below 4 GPa) and above the ordering temperature, as shown in Fig. 1.

For  $\Delta < \Gamma < 2\Delta$ , we have  $T_0 < 150$  K and  $n_f \geq 0.8$ , and still obtain  $S(T)$  with the two maxima. But  $S_{\text{max}}$  is now positive, the value of  $S_0$  is enhanced, the temperature interval in which  $S(T) < 0$  is reduced, and  $S(T)$  at the minimum is less negative than for smaller  $\Gamma$ . As we increase  $\Gamma$  (by increasing pressure), the sign-change of  $S(T)$  is removed,  $S_0$  and  $S_{\text{max}}$  are further enhanced, but  $T_S$  is not changed. The two peaks are coming closer together and are merging eventually. These features are typical of Kondo systems with moderate  $T_0$ , say  $T_0 \geq 10$  K, and are in a qualitative agreement with the data on the type (b) and (c) systems mentioned in Sec. I. They are also shown by the  $\text{CeRu}_2\text{Ge}_2$  data<sup>11</sup> at intermediate pressures, (see the curves in Fig. 1 for pressure above 3.4 GPa.)

At  $\Gamma \approx 2\Delta$ , the system enters the VF regime,  $S(T)$  acquires a single maximum at  $T_S$ , with a shoulder on the low-temperature side. Even this shoulder vanishes, when  $\Gamma$  is increased further, as shown in Fig. 3. For  $\Gamma > 2\Delta$  the thermopower is of the type (d), with a single peak which is much steeper on the high- than on the low-temperature side. This peak shifts to higher temperatures with increasing  $\Gamma$  (pressure) and  $S_{\text{max}}$  saturates (see inset to Fig. 3); the initial slope of  $S(T)$  decreases continuously with  $\Gamma$ . Such a behavior is in a qualitative agreement with the thermopower data on valence fluctuators<sup>16,17,18</sup> and with the high-pressure data on  $\text{CeRu}_2\text{Ge}_2$ <sup>11</sup> (cf. inset to Fig. 1) and  $\text{CeCu}_2\text{Si}_2$ <sup>5</sup>. However, a large discrepancy appears between theory and experiment at low

temperatures, because  $A(\omega)$  is overestimated for  $\omega \simeq 0$ , which makes the NCA curves larger than the experimental ones. A possible correction of the initial  $S(T)/T$  values is discussed below.

The  $f$ -electron number  $n_f$ , calculated for the parameters used in Figs. 2 and 3, is plotted in Fig. 4 as a function of temperature. The overall temperature dependence is rather slow, but two different types of behavior can still be seen. For  $\Gamma < 2\Delta \ll -E_f$ , we find that  $n_f$  is nearly independent of temperature and close to 1, which is typical of Kondo systems.<sup>36</sup> For  $\Gamma > 2\Delta$ , we find that  $n_f$  is less than 0.8 and nearly constant at low temperatures but at about  $T \simeq \Delta/3k_B$  (271 K for  $\Delta=0.07$  eV) there is an increase followed by the saturation at high temperatures. Considered as a function of  $\Gamma$  (pressure),  $n_f(\Gamma)$  shows different behavior at high and low temperatures. At high temperatures  $n_f$  decreases uniformly as  $\Gamma$  increases. At low temperatures  $n_f$  does not change much for  $\Gamma \ll \Delta$  and  $\Gamma \gg \Delta$ , but drops rapidly around  $\Gamma \simeq 2\Delta$ , indicating the crossover from the Kondo to the VF regime.

The electrical resistivity,  $\rho_{mag}(T)$ , obtained for small and intermediate values of  $\Gamma$ , is shown in Fig. 5. The interesting feature is the high-temperature maximum, which appears for  $\Gamma < \Delta$ , and correlates very well with the maximum in  $S(T)$ . For temperatures below the maximum,  $\rho_{mag}(T)$  drops to a minimum and then rises logarithmically as  $T_0$  is approached. This minimum and the subsequent low-temperature upturn are of a purely electronic origin and appear in systems with small  $T_0$  and large CF splitting. In these systems, one can follow the evolution of the two peaks in  $\rho_{mag}(T)$ , and observe the disappearance of the minimum with the application of pressure. For example, in CeRu<sub>2</sub>Ge<sub>2</sub>,<sup>11</sup> CePd<sub>2</sub>Ge<sub>2</sub>,<sup>37</sup> CePd<sub>2</sub>Si<sub>2</sub>,<sup>38</sup> or CeCu<sub>5</sub>Au<sup>39</sup> the minimum becomes more shallow, transforms into a shoulder, and vanishes at high enough pressure. As discussed already, the NCA overestimates the low-temperature scattering and distorts the relative magnitude of the high- and low-temperature peaks. In addition, the single-ion approximation always gives  $\rho_{mag}(T)$  which saturates at low temperature and cannot explain the low-temperature reduction of  $\rho_{mag}(T)$ , which is seen in stoichiometric compounds below the onset of coherence. The electrical resistance of Ce-based Kondo systems at very high pressure, and the ambient pressure data of valence fluctuators, cannot be described by the NCA solution. In these systems, the scattering on  $f$  ions remains coherent up to rather high temperatures and the NCA solution is valid only above the high-temperature maximum and is not physically relevant.

To illustrate the situation in Yb intermetallics, we perform a generic calculation for a semielliptical (hole) conduction band and four CF doublets. The NCA equations are solved for a single  $f$  hole ( $\mathcal{N} = 8$ ). Following the procedure outlined in Sec. II, we start the calculations at ambient pressure and temperature  $T_\Delta$ , such that the  $f$  state is almost free, and calculate  $n_{tot}^{hole} = n_c^{hole} + n_f^{hole}$  for

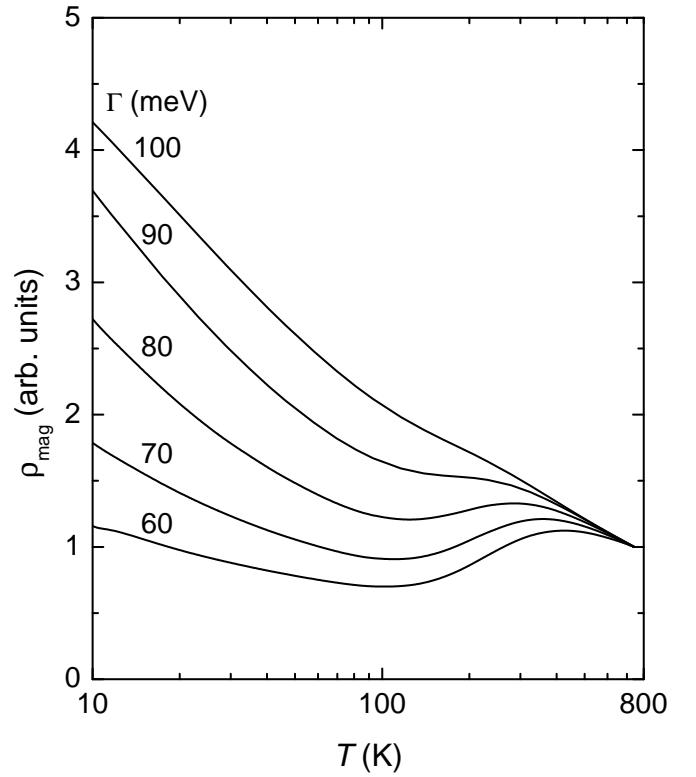


FIG. 5: Electrical resistivity vs. temperature calculated by the NCA for the CF splitting  $\Delta = 0.07$  eV and for several values of the hybridization strength  $\Gamma$ , as indicated in the figure.

the initial parameter set  $\{W, E_c^0, N, \Gamma, E_f^0, \Delta_i, \mathcal{N}_i\}$ . At lower temperatures we shift  $E_c$  and  $E_f$  with respect to  $E_c^0$  and  $E_f^0$  by  $\delta\mu$ , so as to conserve  $n_{tot}^{hole}$ , and calculate the response functions for this new parameter set; this procedure does not change  $E_c - E_f$ . At a higher pressure, we start again at  $T = T_\Delta$ , change  $E_f$  so as to increase  $n_f^{hole}$  and find  $E_c$  which conserves  $n_{tot}^{hole}$ . Since  $\Gamma$  is not changed by this procedure, we now have  $E_c - E_f \neq E_c^0 - E_f^0$ . For temperatures below  $T_\Delta$ , the properties of the system are calculated by the same procedure as at ambient pressure, i.e.,  $n_{tot}^{hole}$  is conserved by shifting  $E_c$  and  $E_f$  by the same amount  $\delta\mu$ .

Taking  $W = 4$  eV,  $E_c^0 = 1.0$  eV,  $\Gamma=0.08$  eV,  $E_f^0 = -0.8$  eV, and three excited CF doublets at  $\Delta_1=0.02$  eV,  $\Delta_2=0.04$  eV,  $\Delta_3=0.08$  eV, respectively, we find  $n_{tot} = 6.444$  at  $T = T_\Delta$ . The  $S(T)$  obtained for  $E_f$  ranging from  $E_f = -0.6$  eV to  $E_f = -1.0$  eV, is shown in Fig. 6. We recall, that an increase of pressure makes  $E_f$  more negative. For  $E_f = -0.6$  eV, the thermopower shows a deep minimum, typical of Yb ions in the VF state. For  $E_f = -0.8$  eV,  $S(T)$  develops a small maximum, which separates the high-temperature minimum at  $T_S$  and the low-temperature minimum at  $T_0$ . By making  $E_f$  more negative we shift  $T_0$  to lower values, as shown in Fig. 6 by the curves obtained for  $E_f = -0.8$  eV,  $E_f = -0.85$  eV, and  $E_f = -0.9$  eV, respectively. The low-temperature



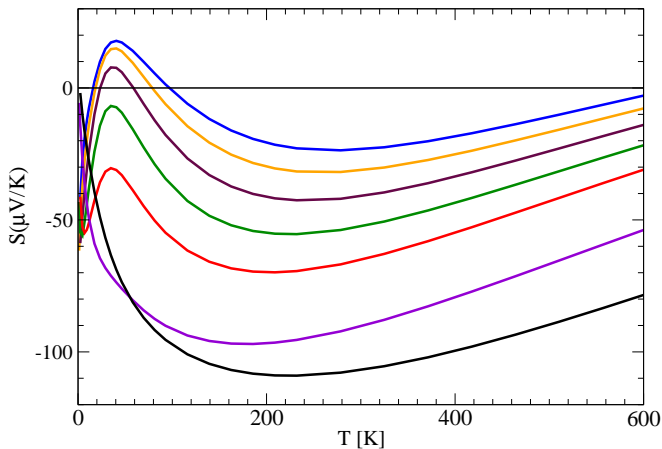


FIG. 6: Thermopower due to Yb ions, obtained by the NCA for four CF doublets, is plotted as a function of temperature for various values of  $E_f^0$ , i.e. for various pressures. Starting from the uppermost curve, we show  $S(T)$  for  $-E_f^0=1.00; 0.95; 0.90; 0.85; 0.80; 0.70$ , and  $0.60$  eV, respectively. The bottom curve ( $E_f^0=-0.6$  eV) corresponds to the lowest pressure.

range in which  $S(T)$  is negative shrinks with pressure, in agreement with the experimental data.<sup>30</sup> However, for  $E_f$  much below  $\mu$ , the NCA calculations break down before this minimum is reached. As regards the value of  $S(T)$  at the maximum, it is negative at first but it becomes positive as pressure increases, i.e., the thermopower changes from (c)-type to (b)-type. At very high pressures, such that the  $n_{tot}^{hole} \simeq 1$ , the thermopower is dominated at low temperatures by a large positive peak and at high temperatures by a negative minimum, which is typical of Yb-based systems with a small Kondo scale. The shape of  $S(T)$  is directly related to the magnetic character of Yb ions and our calculations explain the qualitative features of the thermopower of YbAu<sub>2</sub>, YbAu<sub>3</sub>,<sup>29</sup> and YbSi, YbNi<sub>2</sub>Si<sub>2</sub>,<sup>30</sup> which are of the (a)-type, of Yb<sub>2</sub>Ir<sub>3</sub>Al<sub>9</sub>,<sup>32</sup> YbAuCu<sub>4</sub>,<sup>31</sup> and YbNiSn,<sup>30</sup> which are of the (b)-type, of YbPdCu<sub>4</sub>,<sup>31</sup> and Yb<sub>2</sub>Rh<sub>3</sub>Al<sub>9</sub>,<sup>32</sup> which are of the (c)-type, and of YbAgCu<sub>4</sub>, YbPd<sub>2</sub>Cu<sub>2</sub>,<sup>31</sup> and YbInAu<sub>2</sub><sup>30</sup> which are (d)-type. The pressure effects in YbSi,<sup>30</sup> and the chemical pressure effects in YbCu<sub>2</sub>Si<sub>2</sub><sup>33</sup> are also in a qualitative agreement with our results.

An estimate of the low-temperature properties of the single-impurity model can be obtained by combining the NCA results with the universal FL laws. The Sommerfeld expansion of transport coefficients in Eq.(4) gives<sup>45</sup>

$$\lim_{T \rightarrow 0} \frac{\Gamma S(T)}{k_B T} = \frac{\pi^2 k_B}{3|e|} \sin\left(\frac{2\pi}{\mathcal{N}_0} n_f\right) Z, \quad (6)$$

where  $\pi^2 k_B / 3|e| = 283.5$   $\mu\text{V/K}$  and  $Z$  is the enhancement factor defined by the Fermi-level derivative of the  $f$ -electron self-energy,  $Z = [1 - \partial\Sigma/\partial\omega]_{\omega=T=0}$ .  $\Gamma/Z$  is related to the Kondo scale by a factor of order 1. Setting  $T_0 = \Gamma/Z$ , and using for  $n_f(T=0)$  the NCA results of Fig. 4, we can estimate from Eq.(6) the initial slope of the curves plotted in Figs. 2 and 3. The obtained

values, which go from 32  $\mu\text{V/K}^2$  for  $\Gamma=60$  meV to 1  $\mu\text{V/K}^2$  for  $\Gamma=130$  meV and 0.1  $\mu\text{V/K}^2$  for  $\Gamma=200$  meV, are in the range reported recently for various Ce-based heavy fermions and valence fluctuators (see Table 1 in ref. <sup>12</sup>). The initial slope of  $S(T)$  decreases as we move from the Kondo to the VF limit, in agreement with pressure experiments.<sup>11</sup> At higher temperatures, the non-linear corrections reduce  $S(T)$  and give rise to a maximum at  $T_0$ . These non-linear corrections are non-universal, and a large slope does not necessary translate into large  $S(T)$  at  $T_0$ . The corresponding calculations for the Yb curves plotted in Fig. 6 show that an application of pressure enhances  $S(T)/T$ .

The initial slope of  $S(T)$  can also be related to the  $\gamma$  coefficient of the specific heat, with the important result that the ratio  $S(T)/\gamma T = (2\pi/|e|\mathcal{N}_0)\cot(\pi n_f/\mathcal{N}_0)$  is independent of  $Z$ . This expression and Eq.(6) are valid in the single-impurity regime, and it is not obvious that they would produce the correct results for stoichiometric compounds. However, the characteristic energy scales of a coherent FL (inferred from the experimental data on the initial slope of the thermopower, or the specific heat coefficient) do not seem to be much different from the single-ion scale  $T_0$  of the LM regime (inferred, say, from the peak in the thermopower or the Curie-Weiss temperature).

#### IV. DISCUSSION OF SPECTRAL PROPERTIES

In this section we present the NCA results for  $A(\omega)$ , study the low-energy spectral features in the vicinity of various fixed points, discuss the changes induced by the crossovers, and explain the behavior of  $S(T)$  in terms of the redistribution of spectral weight within the Fermi window (F window). Only the Ce case is considered and it is assumed that pressure gives rise to an increase of the hybridization width  $\Gamma$ . The results obtained for  $\Gamma < \Delta$  are shown in Fig. 7, where  $A(\omega)$  is plotted as a function of frequency for several temperatures. At high temperatures,  $T \simeq T_\Delta$ , the spectral function has a broad charge-excitation peak somewhat above  $E_f$  and a narrower resonance of half-width  $\Delta$ , centered below  $\mu$ . This low-energy resonance is a many-body effect due to the hybridization of the conduction states with the  $4f$  states and is typical of the exchange scattering on the full multiplet. In this temperature range, the F window shows more spectral weight below than above  $\mu$  (see the middle panel in Fig. 7) and  $S(T) < 0$ . The magnetic susceptibility<sup>43</sup> is Curie-Weiss like, with a very small Curie-Weiss temperature and a Curie constant which is close to the free Ce ion value. The maximum of  $S(T)$  at about  $T_S \simeq T_\Delta/2$  is here negative,  $S_{max} < 0$ , but a slight increase of  $\Gamma$  would make  $S_{max}$  positive. All these features are typical of the LM fixed point corresponding to a fully degenerate  $f$ -state. At lower temperatures,  $T < T_S$ , the CF splits the many-body resonance into two peaks. The larger one grows below  $\mu$  and the smaller one above  $\mu$  (see the



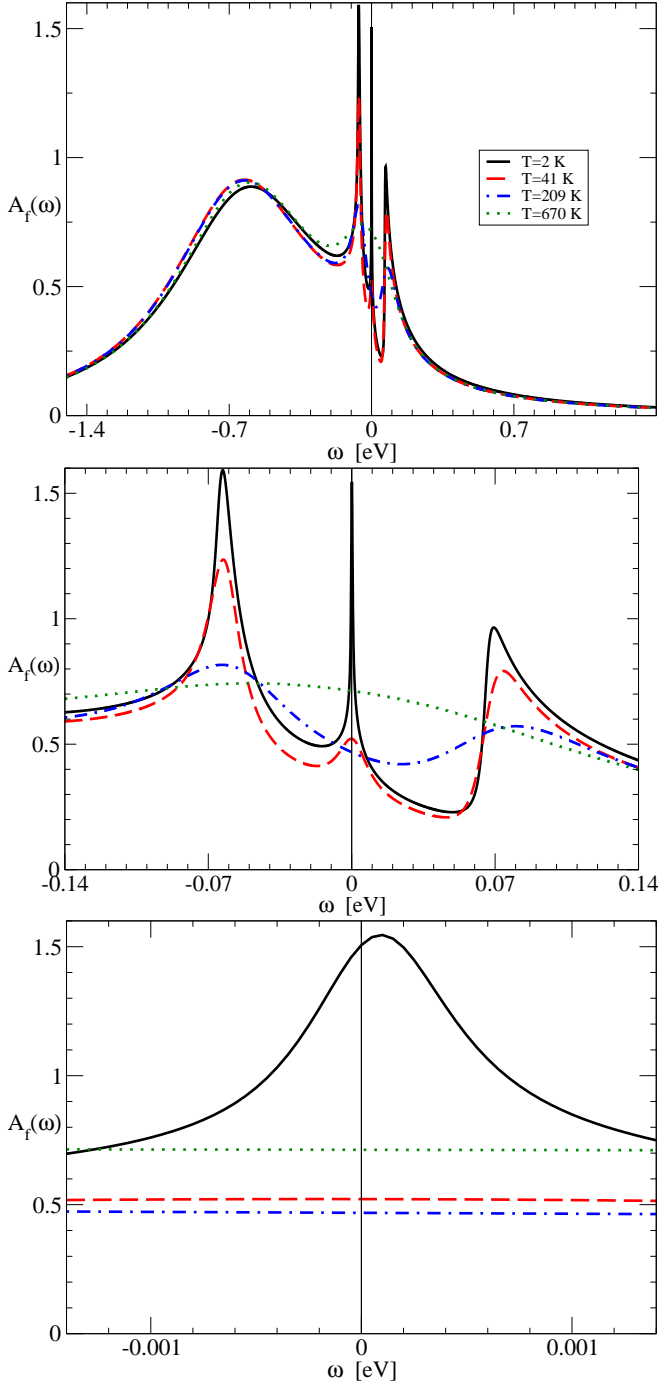


FIG. 7: Spectral function  $A(\omega)$ , calculated for the hybridization strength  $\Gamma=0.06$  eV and the CF splitting  $\Delta=0.07$  eV, plotted as a function of frequency for several temperatures. The solid, dashed, dashed-dotted and dotted curves correspond to  $T = 2, 41, 209$ , and  $670$  K, respectively. The charge-excitation peak is visible in the upper panel. The middle panel shows the evolution of the CF and Kondo resonances with temperature. For  $T \leq \Delta$ , the many-body resonance of half-width  $\Delta$  is centered well below  $\mu$ . The F window has more states below than above  $\mu$  and  $S(T) < 0$ . The lower panel shows the position of the Kondo resonance above  $\mu$ . Its center defines  $T_0 = 1$  K. For  $T \leq T_0$  the F window has more states above than below  $\mu$  and  $S(T) > 0$ .

middle panel in Fig. 7). This asymmetry is enhanced as  $\Gamma$  is reduced, which is typical of the Anderson model with CF splittings;<sup>43</sup> the increase of the low-energy spectral weight below  $\mu$  gives rise to a large negative thermopower. A further reduction of temperature leads, for  $T \ll T_\Delta$ , to a rapid growth of an additional peak very close to  $\mu$ , such that  $A(\omega)$  acquires three pronounced low-energy peaks (see Fig. 7). (The physical origin of these many-body resonances is explained in detail in Ref.<sup>43</sup>) The peak centered at  $\omega_0 \ll \Delta$  is the Kondo resonance and its appearance below  $T \leq 40$  K marks the onset of the LM regime, which is due to scattering of conduction electrons on the lowest CF level. The two CF peaks centered at about  $\omega_0 \pm \Delta$  are outside the F window, and do not affect the low-temperature transport and thermodynamics. Once the Kondo peak appears, the F window shows more spectral weight above than below  $\mu$  and  $S(T)$  is positive, which is just the opposite to what one finds for  $T \geq T_\Delta$ . The center of the Kondo resonance saturates at low temperatures at the energy  $\omega_0 > 0$ , which provides the NCA definition of the Kondo scale,  $k_B T_0 = \omega_0$ . In the symmetric Anderson model  $T_0$  is related to the width of the Kondo resonance but in the highly asymmetric case we are dealing with here, the current definition is more appropriate. The comparison with numerical renormalization group (NRG) calculations<sup>50</sup> shows that  $\omega_0$  gives a reliable estimate of the Kondo temperature even for a doubly degenerate Anderson model, and we assume that the NCA definition of  $T_0$  provides the correct Kondo scale of the CF-split single-impurity Anderson model as well. Because the Kondo resonance is asymmetric with respect to the  $\omega = 0$  line and has more states above than below  $\mu$ , the reduction of temperature enhances  $S(T)$  until it reaches, at  $T_0$ , the maximum value  $S_0$ . A further temperature reduction leaves the top of the Kondo resonance outside the F window, and the thermopower drops. However, most Ce and Yb system with very small  $T_0$  have a phase transition above  $T_0$ , and to discuss the normal-state properties of (a)-type systems it is sufficient to consider the NCA solution for  $T \geq T_0$ .

An increase of the coupling to  $\Gamma > \Delta$  has a drastic effect on  $A(\omega)$ , as illustrated in Fig. 8, where  $A(\omega)$  is plotted for  $\Gamma = 0.12$  eV. The charge-excitation peak is transformed into a broad background (see the upper panel in Fig. 8) and the only prominent feature at  $T \simeq T_\Delta$  is the low-energy resonance of half-width  $\Delta$  centered above  $\mu$ . This low-energy resonance is due to the exchange scattering of conduction electrons on the full CF multiplet, which gives rise to the maximum of  $S(T)$  in the LM regime. The F window (see lower panel in Fig. 8) shows more spectral weight above than below  $\mu$ , so that  $S(T) > 0$ . The reduction of temperature below  $T_S$  removes some spectral weight above  $\mu$  and brings additional spectral weight below  $\mu$ , which reduces  $S(T)$  and leads to a minimum.<sup>51</sup> A further reduction of temperature leads to the rapid growth of the Kondo peak at  $\omega_0$ , and the CF peak at  $\omega_0 + \Delta$ , but the negative CF peak

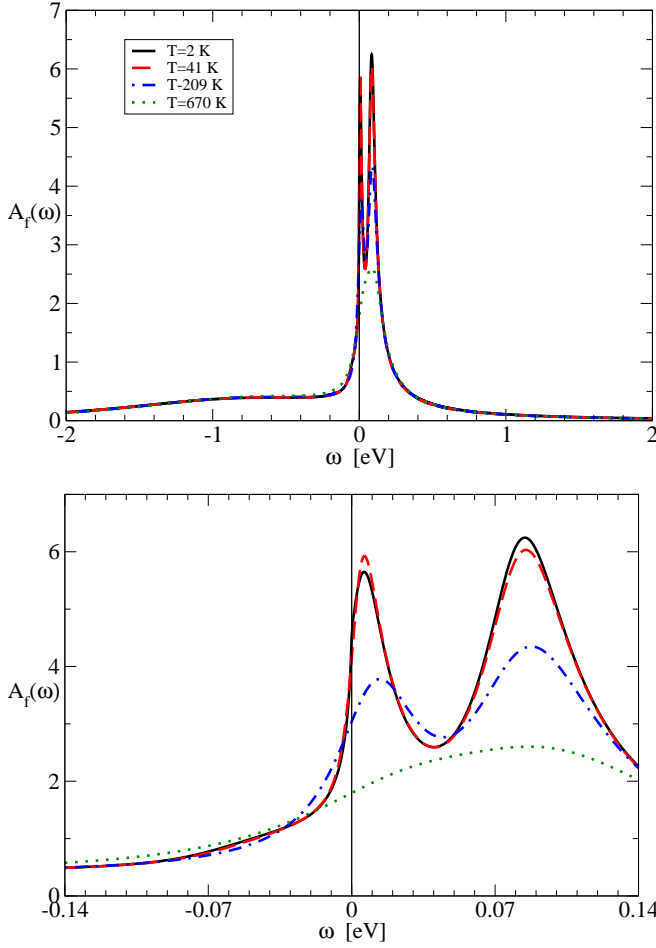


FIG. 8: Spectral function  $A(\omega)$ , calculated for the hybridization strength  $\Gamma=0.12$  eV and the CF splitting  $\Delta=0.07$  eV, plotted as a function of frequency for several temperatures. The solid, dashed, dashed-dotted and dotted curves correspond to  $T = 2, 41, 209$ , and  $670$  K, respectively. The upper panel shows the overall features. The two many body resonances are resolved but the lower CF peak and the charge-excitation peak are absent. The lower panel shows the evolution of low-energy resonances with temperature. For  $\Gamma > \Delta$ , there is more spectral weight above than below  $\mu$  at all temperatures and  $S(T)$  is always positive.

does not develop. That is, an increase of pressure removes the lower CF peak, and shifts the Kondo and the upper CF peak to higher energies, without changing their separation  $\Delta$ . The F window shows more spectral weight above than below  $\mu$ , so that  $S(T)$  is positive and grows as temperature is lowered. The maximum  $S_0$  is reached at  $T_0$  when the Kondo resonance is fully developed. The characteristic energy scale is defined again by the position of the Kondo peak,  $k_B T_0 = \omega_0$ , which can now be quite large. For  $T \leq T_0$  the F window becomes narrower than the Kondo resonance and  $S(T)$  drops below  $S_0$ . For  $T \ll T_0$ , where the FL behavior is expected,<sup>43</sup> the NCA gives  $A(\omega)$  with an unphysical spike at  $\mu$ , which makes  $\rho_{mag}(T)$  and  $S(T)$  much larger than the exact result.

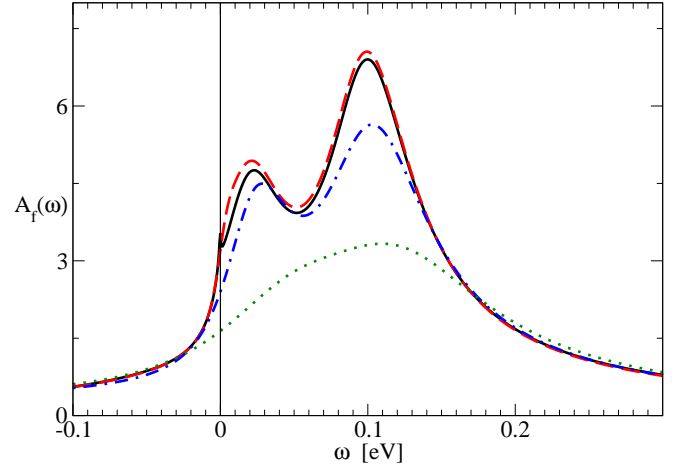


FIG. 9: Spectral function  $A(\omega)$ , calculated for the hybridization strength  $\Gamma=0.140$  eV and the CF splitting  $\Delta = 0.07$  eV, plotted as a function of frequency for several temperatures. The solid, dashed, dashed-dotted and dotted curves correspond to  $T=2, 41, 209$ , and  $670$  K, respectively. For  $\Gamma > \Delta$ , the Kondo resonance is reduced to a small hump above the  $f$  level.

However, once  $T_0$  is obtained from the NCA calculations, the low-temperature transport can be inferred from the universal power laws which hold in the FL regime, as discussed in the previous section.

A further increase of  $\Gamma$  shifts the Kondo and the CF peaks to higher energies, and changes their relative spectral weight, as shown in Fig. 9, where the low-frequency part of  $A(\omega)$  is shown for  $\Gamma = 2\Delta$ . The Kondo scale is still defined by the center of the Kondo peak, even though it is now reduced to a hump on the low-energy side of a large peak centered at  $\omega_0 + \Delta$ . The unphysical NCA spike at  $\omega = 0$  can be seen at lowest temperatures. The thermopower is positive at all temperatures and has only a shoulder below  $T_S$ . A quantitative comparison between  $T_0$ , defined by the position of the Kondo resonance, and the position of the Kondo anomaly in  $S(T)$  becomes difficult.

Finally, for  $\Gamma > 2\Delta$ , we find  $A(\omega)$  with a single broad peak centred at  $\tilde{E}_f > 0$ , as shown in Fig. 10. The CF excitations are now absent, which is typical for the Anderson model in the vicinity of the VF fixed point. The relevant energy scale at low temperature is defined as  $k_B T_0 = \tilde{E}_f$ , and shows an almost linear dependence on  $\Gamma$ . The thermopower is always positive and grows monotonically from small values at low temperatures towards a high-temperature maximum at  $T_S$ . The unphysical spike at  $\omega = 0$  appears at higher temperatures and is more pronounced than for small  $\Gamma$ , as illustrated in Fig. 10. The initial slope of  $S(T)$  obtained from the NCA result for transport coefficients is very much overestimated with respect to the FL result based on Eq.(6). An increase of temperature above  $T_S$  modifies the excitation spectrum on an energy scale of the order of  $\tilde{E}_f$  and reduces  $S(T)$ . The values of  $\tilde{E}_f$  and  $T_S$  do not seem to be related in any

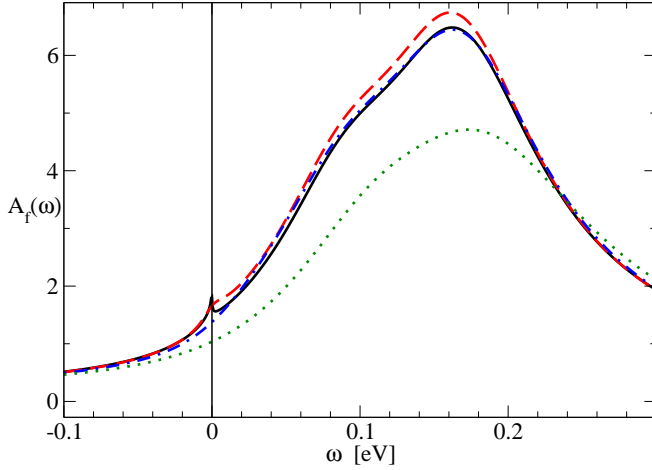


FIG. 10: Spectral function  $A(\omega)$ , calculated for the hybridization strength  $\Gamma=0.20$  eV and the CF splitting  $\Delta = 0.07$  eV, plotted as a function of frequency for several temperatures. The solid, dashed, dashed-dotted and dotted curves correspond to  $T=2, 41, 209$ , and  $670$  K, respectively. For  $\Gamma \gg \Delta$ , the Kondo resonance is absent.

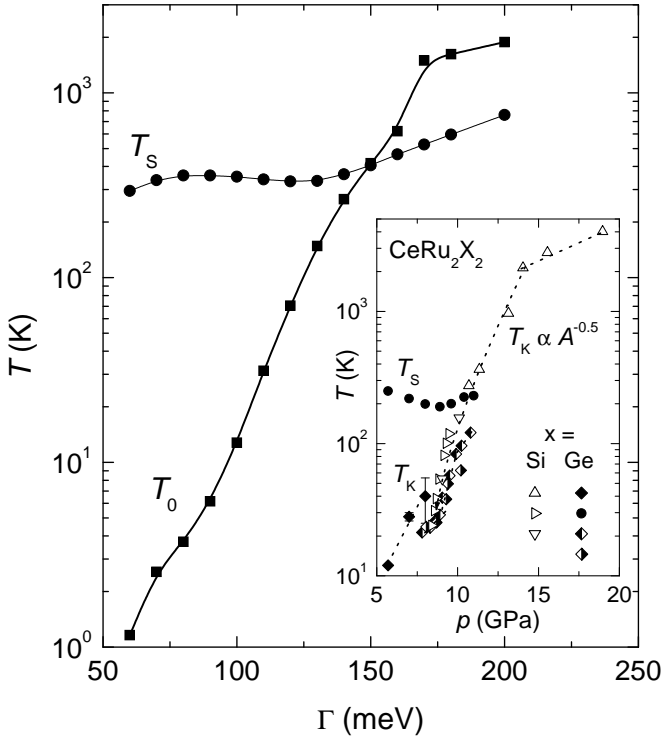


FIG. 11: The temperature  $T_S$ , defined by the high-temperature maximum of the thermopower, and the characteristic scale  $T_0$ , defined by the peaks in the spectral function, are plotted as functions of the hybridization strength  $\Gamma$ . The three regions, where  $T_0$  changes its functional form, are clearly seen. The inset reproduces the experimental data for  $\text{CeRu}_2\text{Ge}_2$  and  $\text{CeCu}_2\text{Ge}_2$ .<sup>11</sup>

simple way, and the temperature-induced breakdown of the local FL is not indicated by any FL scale. An increase of  $\Gamma$  (pressure) changes  $A(\omega)$  and enhances  $T_S$  but does not lead to further enhancement of  $S_{max}$ . The pressure dependence of  $\tilde{E}_f$  and  $T_S$  looks different. In other words, the description of the VF regime requires more than one energy scale.

The characteristic scales of the Anderson model obtained for various values of  $\Gamma$  provide the  $(T, p)$  phase diagram of the system plotted in Fig. 11. The  $T_0$  line is defined by the position of the Kondo peak and the  $T_S$ -line by  $S_{max}$ . At small  $\Gamma$  (low pressure) Fig. 11 indicates two crossovers. The one around  $T_0$  is between the FL and the LM regime defined by the lowest CF level. The one around  $T_S$  is the crossover to the high-temperature LM regime, as defined by a full CF multiplet. When these LM regimes are well separated, the crossover between them is accompanied by a minimum and, possibly, a sign-change of  $S(T)$ . At intermediate pressures, the two LM regimes are too close for the sign-change to occur, and the crossover is indicated only by a shallow minimum or just a shoulder of  $S(T)$ . Here, the relationship between the low-temperature maximum of  $S(T)$  and the center of the Kondo peak can only be given as an order-of-magnitude estimate. At very high pressures, the system is in the VF regime and the crossover from a universal low-temperature FL phase to a non-universal high-temperature phase takes place at  $T \simeq T_S$ . This crossover is not defined by the FL scale  $\tilde{E}_f$ , which is very large, but by a much smaller scale  $T_S$ .

## V. CONCLUSIONS AND SUMMARY

We have applied the single-impurity Anderson model to the investigation of the temperature and pressure dependence of the thermopower of Ce and Yb intermetallics, and found that the crossovers between various fixed points explain the seemingly complicated temperature dependence of  $S(T)$ .

The basic assumption of our approach is that for a given concentration of rare-earth ions, and above some coherence temperature, the system is in an "effective impurity" regime. In that "impurity limit", we treat the rare-earth ions as independent scattering centers and solve the ensuing single-impurity model by the NCA. Our calculations impose the charge neutrality constraint on the local scattering problem, which provides a minimal self-consistency condition for describing the pressure effects. The excitation spectrum obtained in such a way is very sensitive to the changes in the coupling constant  $g = \Gamma/\pi|E_f|$ , and an increase of the hybridization or a shift of the  $f$  state, which modifies the magnetic state of the  $f$  ion, has a huge effect on the spectral function. Since the excitation spectrum is related to the transport coefficients by Kubo formulas, the thermopower changes rapidly as a function of temperature, pressure or doping. The shapes (a) to (d) assumed by  $S(T)$  in various regions

of the parameter space follow straightforwardly from the redistribution of the single-particle spectral weight within the Fermi window.

The NCA solution of the single-impurity Anderson model breaks down for  $T < T_0$ . However, the excitations above the ground state are determined by the general FL laws, which can be used to find the initial slope of  $S(T)$ . Estimating the Kondo scale and the number of  $f$  electrons by the NCA calculations, we find that an increase of pressure reduces (enhances) the low-temperature value of  $S(T)/T$  in Ce (Yb) compounds. Combining the FL and the NCA results, we can obtain  $S(T)$  in the full temperature range at any pressure.

Our results explain the thermopower of most intermetallic Ce compounds mentioned in Section I. The multi-peaked  $S(T)$ , which characterizes the type (a) and (b) systems, is obtained for Kondo ions with small  $T_0$  and well-defined CF resonances. A type (c) thermopower, which has weakly resolved peaks or just a broad hump, is obtained for Kondo ions with large  $T_0$  and partially overlapping CF resonances. A single-peaked  $S(T)$  of the (d)-type is obtained for the VF ions which do not show any CF splitting of the single-particle excitations. If we assume that pressure increases  $\Gamma$ , and reduces  $n_f$ , our results account for the changes of  $T_0$ ,  $S_0$ ,  $S(T)/T$ , and  $S_{max}$ , observed in pressure experiments on Ce compounds.<sup>2,11,19,20,21,22,23</sup> The strong doping dependence<sup>1</sup> of  $S(T)$  is explained as a chemical pressure effect, which changes the  $f$  occupation. In our local model the "effective concentration" of  $f$  electrons is determined self-consistently, and the thermopower of concentrated and dilute systems cannot be related by simple scaling. (Just like the high pressure data cannot be described in terms of rescaled ambient pressure data.) The relevant energy scales obtained for different values of  $\Gamma$  agree with the  $(T, p)$  phase diagram of CeRu<sub>2</sub>Ge<sub>2</sub> and CeCu<sub>2</sub>Ge<sub>2</sub>, inferred from the high-pressure transport and thermodynamic data.<sup>11</sup>

For Yb compounds, we argue that pressure or chemical pressure mainly affect the position of the crystal field levels relative to the band center, while leaving the hybridization width unchanged. By shifting  $E_f$ , so as to

increase the number of holes, we obtain the thermopower of the type (a) to (d), in agreement with the experimental data. The qualitative features seen in Yb intermetallics at various pressures or chemical pressures are captured as well,<sup>29,30,31,32,33</sup> but different compounds require different initial parameters, and a detailed analysis is yet to be done.

In summary, the normal-state properties of stoichiometric compounds with Ce and Yb ions seem to be very well described by the local model which takes into account spin and charge fluctuations. The classification of the thermopower data follows straightforwardly from the fixed point analysis of the single-impurity Anderson model with the CF splitting. A rich variety of shapes assumed by  $S(T)$  at various pressures or doping dramatically illustrates the effect of the local environment on the response of the single rare earth ion. The nature of the ground state, and the fact that the ground state of many Ce and Yb systems can be changed with pressure or doping, do not seem to affect the thermopower in the normal state. We take this as an indication that the normal state properties of Ce and Yb compounds are dominated by the local dynamics.

The main problem with our poor man's treatment of ordered compounds is that it neglects the coherent scattering which sets in at low enough temperatures, and reduces the thermopower below the values predicted by the local Fermi liquid theory. We can argue that these effects do not change the qualitative features of the thermopower but the proper answer cannot be obtained without solving the lattice model.

### Acknowledgements

We acknowledge useful comments and suggestions from B. Coqblin, J. Freericks, C. Geibel, A. Hewson, B. Horvatić, and H. Wilhelm. This work has been supported by the Ministry of Science of Croatia (CRO-US joint projects, grant number 1/2003, by the National Science Foundation under grant number DMR-0210717, and the Swiss National Science Foundation under grant number 7KRPJ065554-01/1.

- 
- <sup>1</sup> J. Sakurai, H. Takagi, S. Taniguchi, T. Kuwal, Y. Isikawa, and J.-L. Tholance, J. Phys. Soc. Japan **65**, Suppl. B, 49 (1996).
  - <sup>2</sup> P. Link, D. Jaccard, and P. Lejay, Physica B **225**, 207 (1996).
  - <sup>3</sup> V. Zlatić et al, Phys. Rev. B **68**, 104432 (2003).
  - <sup>4</sup> G. Sparn, W. Lieka, U. Gottwick, F. Steglich, and N. Grewe, J. Magn. Magn. Mater. **47 & 48**, 521 (1985).
  - <sup>5</sup> D. Jaccard, J. M. Mignot, B. Bellarbi, A. Benoit, H. F. Braun, and J. Sierro, J. Magn. Magn. Mater. **47 & 48**, 23 (1985).
  - <sup>6</sup> D. Huo, T. Kuwai, T. Mizushima, Y. Isikawa, and J. Sakurai, Physica B **312 & 313**, 232 (2002).
  - <sup>7</sup> D. Huo, K. Mori, T. Kuwai, S. Fukuda, Y. Isikawa, and J.

- Sakurai, Physica B **281 & 282**, 101 (2000).
- <sup>8</sup> J. Sakurai, D. Huo, D. Kato, T. Kuwai, Y. Isikawa, and K. Mori, Physica B **281 & 282**, 98 (2000).
- <sup>9</sup> P. B. van Aken, H. J. van Daal, and K. H. J. Buschow, Phys. Lett. A **49**, 201 (1974).
- <sup>10</sup> R. Cibir, D. Jaccard, and J. Sierro, J. Magn. Magn. Mater. **108**, 107 (1992).
- <sup>11</sup> H. Wilhelm and D. Jaccard, Phys. Rev. B **69**, 214408 (2004).
- <sup>12</sup> K. Behnia, D. Jaccard, and J. Flouquet, J. Phys.: Cond. Matt., **16**, 5187 (2004).
- <sup>13</sup> F. Steglich, Festkörperprobleme XVII, 319 (1977).
- <sup>14</sup> J. Sakurai, J. C. Gomez Sal, and J. Rodriguez Fernandez, J. Magn. Magn. Mater. **140 - 144**, 1223 (1995).

- <sup>15</sup> A. Amato, D. Jaccard, J. Sierro, P. Haen, P. Lejay, and J. Flouquet, *J. Low. temp. Phys.* **77**, 195 (1989).
- <sup>16</sup> Y. Ōnuki and T. Komatsubara, *J. Magn. Magn. Mater.* **63 & 64**, 281 (1987).
- <sup>17</sup> J. Sakurai, T. Ohyama, and Y. Komura, *J. Magn. Magn. Mater.* **47 & 48**, 320 (1985).
- <sup>18</sup> E. Bauer, *Adv. Phys.* **40**, 417 (1991).
- <sup>19</sup> C. Fierz, D. Jaccard, and J. Sierro, *J. Appl. Phys.* **63**, 3899 (1988).
- <sup>20</sup> D. Jaccard, K. Behnia and J. Sierro, *Phys. Lett. A* **163**, 475 (1992).
- <sup>21</sup> D. Jaccard, J. M. Mignot, B. Bellarbi, A. Benoit, H. F. Braun, and J. Sierro, *J. Magn. Magn. Mater.* **47&48**, 23 (1985).
- <sup>22</sup> P. Link, D. Jaccard, and P. Lejay, *Physica B* **225**, 207 (1996).
- <sup>23</sup> P. Link, D. Jaccard, and P. Lejay, *Physica B* **223&224**, 303 (1996).
- <sup>24</sup> Y. Bando, J. Sakurai, and E. V. Sampathkumaran, *Physica B* **186 - 188**, 525 (1993).
- <sup>25</sup> E. Gratz, E. Bauer, R. Hauser, N. Pillmayr, G. Hilscher, H. Müller, and B. Barbara, *J. Magn. Magn. Mater.* **76 & 77**, 275 (1988).
- <sup>26</sup> J. Sakurai, H. Kamimura, and Y. Komura, *J. Magn. Magn. Mater.* **76 & 77**, 287 (1988).
- <sup>27</sup> D. Huo, K. Mori, T. Kuwai, H. Kondo Y. Isikawa, and J. Sakurai, *J. Phys. Soc. Japan* **68**, 3377 (1999). Vol.68 No.10, October, 1999 pp.3377-3382
- <sup>28</sup> M. Očko, C. Geibel, and F. Steglich, *Phys. Rev. B* **64**, 195107-1 (2001).
- <sup>29</sup> G. Nakamoto, T. Nobata, S. Ueda, Y. Nakajima, T. Fujioka, and M. Kurisu, *Physica B* **259 - 261**, 154 (1999).
- <sup>30</sup> K. Alami-Yadri, D. Jaccard, and D. Andreica, *J. Low Temp. Phys.* **114**, 135 (1999).
- <sup>31</sup> R. Casanova, D. Jaccard, C. Marcenat, N. Hamdaoui, and M. J. Besnus, *J. Magn. Magn. Mater.* **90 & 91**, 587 (1990).
- <sup>32</sup> O. Trovarelli, C. Geibel, B. Buschinger, R. Borth, S. Mederle, M. Grosche, G. Sparn, and F. Steglich, *Phys. Rev. B* **60**, 1136 (1999).
- <sup>33</sup> D. Andreica, K. Alami-Yadri, D. Jaccard, A. Amato, and A. Schenk, *Physica B* **259 - 261**, 144 (1999).
- <sup>34</sup> H. J. van Daal, P. B. van Aken, and K. H. J. Buschow, *Phys. Lett. A* **49**, 246 (1974).
- <sup>35</sup> I. Aviani, M. Miljak, V. Zlatic, K.-D. Schotte, C. Geibel, and F. Steglich *Phys. Rev. B* **64**, 184438 (2001)
- <sup>36</sup> For  $\Gamma \ll \Delta$ , such that  $n_f \rightarrow 1$ , the NCA equations break down even before  $T = T_0$  is reached.
- <sup>37</sup> H. Wilhelm and D. Jaccard, *Phys. Rev. B* **66**, 064428 (2002)
- <sup>38</sup> A. Demuer, A. T. Holmes, and D. Jaccard, *J. Phys.: Condens. Matter* **14** L529-L535 (2002)
- <sup>39</sup> H. Wilhelm et al, Science and Technology at High Pressure (Proc. AIRAPT-17) M H Manghnani, W J Nellis and M F Nicol (Hyderabad: Universities Press) p 697 (2000) (Preprint cond-mat/9908442)
- <sup>40</sup> H. Wilhelm et al, preprint, cond-mat/0408280
- <sup>41</sup> B. Cornut and B. Coqblin, *Phys. Rev. B* **5**, 4541 (1972).
- <sup>42</sup> A. K. Bhattacharjee and B. Coqblin, *Phys. Rev. B* **13**, 3441 (1976).
- <sup>43</sup> N. E. Bickers, D. L. Cox, and J.W. Wilkins, *Phys. Rev. B* **36**, 2036 (1987); N. E. Bickers, *Rev. Mod. Phys.* **59**, 845(1987).
- <sup>44</sup> G.D. Mahan, *Many-Particle Physics* (Plenum, New York, 1981).
- <sup>45</sup> T A Costi, A C Hewson and V Zlatic, *J. Phys.: Condens. Matter* **6**, 2519 (1994 )
- <sup>46</sup> The results for two near-by excited doublets are the same.
- <sup>47</sup> R. Monnier, L. Degiorgi, and B. Delley, *Phys. Rev. B* **41**, 573 (1990).
- <sup>48</sup> G. D. Mahan, *Solid State Phys.* **51** , 81 (1998).
- <sup>49</sup> J. Freericks et al., *Phys. Rev. B* **68**, 19512 (2003).
- <sup>50</sup> T. A. Costi, J. Kroha, and P. Wölfe, *Phys. Rev. B* **53**, 1850 (1996). 984,
- <sup>51</sup> For not too large values of  $\Gamma$ , the thermopower at the minimum is negative (see  $\Gamma=90$  meV curve in Fig. 2) but if  $\Gamma$  continues to increase the minimum of  $S(T)$  becomes more shallow and does not extend to negative values (see curves in Fig. 2 obtained for  $\Gamma=100-120$  meV).